JOURNAL OF CATALYSIS 81, 131–141 (1983)

Sintering Kinetics of Silica- and Alumina-Supported Nickel in Hydrogen Atmosphere

CALVIN H. BARTHOLOMEW AND WAYNE L. SORENSEN

BYU Catalysis Laboratory, Department of Chemical Engineering, Brigham Young University, Provo, Utah 84602

Received September 9, 1982; revised December 9, 1982

The sintering kinetics of Ni/SiO_2 and $Ni/\gamma\text{-}Al_2O_3$ catalysts in H_2 atmosphere were studied in the temperature range between 923 and 1023 K. Metal surface areas were measured as a function of time using H_2 chemisorption. BET surface areas, pore size distributions, and metal crystallite size distributions were determined for fresh and sintered catalysts using Argon adsorption and transmission electron microscopy. Loss of nickel surface area occurs as a result of metal crystallite growth and support collapse. The latter is more significant at low temperatures and in the Ni/Al_2O_3 system. Growth of metal crystallites is predominant at high temperatures. Ni/SiO_2 sinters more rapidly than Ni/Al_2O_3 at temperatures above 923 K but less rapidly in H_2 atmosphere compared to He atmosphere (the latter comparison based on data obtained in He from a previous study). Orders of sintering decrease with increasing temperature and time of sintering. The kinetic and TEM data are consistent with a shift in mechanism from crystallite migration to atomic migration with increasing temperature and time of sintering.

INTRODUCTION

Supported nickel catalysts find widespread application in hydrogenation, methanation, and steam reforming reactions. Unfortunately, under high temperature reaction conditions conventional nickel catalysts lose metal surface area quite rapidly. The thermal deactivation of supported nickel may involve one or a combination of the following phenomena: (i) growth of metal crystallites, (ii) collapse of the support, and (iii) reaction of the metal with the support. The first of these processes, the growth of metal crystallites, is referred to as "sintering," although all three can result in loss of metal surface area and must therefore be considered in a study of sintering.

There have been relatively few investigations of sintering of supported nickel (*1–7*). Only three of the previous studies reported kinetic data (*3, 6, 7*). Richardson and Crump (*3*) reported rates of sintering in helium atmosphere based on magnetic granulometry measurements at different temperatures for controlled-pH-deposited Ni/SiO_2. Kuo *et al.* (*6*) reported changes in particle size and particle size distribution of commercial, precipitated Ni/SiO_2 with time and temperature. Bartholomew *et al.* (*7*) determined metal surface area loss with time and temperature in H_2 atmosphere from H_2 adsorption measurements for nickel and nickel bimetallics supported on γ- and α-aluminas. Unfortunately, because of differences in the experimental conditions chosen for study, particularly temperature and sintering atmosphere, and because of substantial differences in the preparation of the catalysts, it is not possible to make quantitative comparisons regarding the stability of nickel on alumina and silica from these previous studies (*3, 6, 7*), nor to determine if the data obtained by X-ray and magnetic techniques for Ni/SiO_2 (*3, 6*) are in quantitative agreement. Furthermore, previous investigations from other laboratories did not properly consider the role of support modifications in the sintering process.

Clearly, it would be worthwhile to have sintering data obtained on the same catalyst, e.g., Ni/SiO_2, by different experimental techniques and in different atmospheres

0021-9517/83 $3.00

for purposes of evaluating the relative strengths and limitations of the different techniques and the effects of sintering atmosphere. It would likewise be worthwhile to obtain sintering data under comparable conditions for nickel on different supports in order to determine the effects of support on the thermal stability of nickel. There are also needs for obtaining quantitative sintering kinetic data for purposes of modeling thermal deactivation during reaction processes and for providing insights into the nature of the sintering mechanism.

This study was undertaken to (i) determine the relative thermal stabilities of well-defined Ni/Al_2O_3 and Ni/SiO_2 catalysts in reducing (H_2) atmosphere, (ii) ascertain the contributions of nickel crystallite growth and support collapse to the sintering process, and (iii) provide quantitative kinetic data for modeling the thermal deactivation of these two catalyst types in reducing environment. The sintering experiments were carried out using Ni/Al_2O_3 and Ni/SiO_2 samples having very similar physical properties, e.g., dispersions, particle size distributions, and support surface areas. Fortuitously, the conditions of temperature chosen for this study intersected those of the two previous kinetic studies of Ni/SiO_2 from other laboratories (*3, 6*); moreover the pH-deposited Ni/SiO_2 catalyst used in this study was almost identical to that used by Richardson and Crump (*3*). Accordingly the kinetic data for Ni/SiO_2 from this study can be compared qualitatively and to some extent quantitatively with those obtained using different techniques (*3, 6*) and a different atmosphere (*3*).

EXPERIMENTAL

Catalyst Preparation

The preparation of 13.5% Ni/SiO_2 and 15% Ni/Al_2O_3 catalysts was previously described (*2, 8*). The Ni/SiO_2 catalyst was prepared by a controlled-pH urea deposition–precipitation technique (*3, 9*) using analytically pure $Ni[NO_3]_2 \cdot 6H_2O$ and silica (Cab-O-Sil, Cabot Corporation, M-5, 200 m^2/g) that had been calcined at 873 K for 2 hr previous to the precipitation. The Ni/Al_2O_3 catalyst was prepared using a simple impregnation with an aqueous solution of nickel nitrate (*2, 8*) of γ-alumina (Kaiser SAS 5×8 mesh), which had been calcined at 873 K for 2 hr (BET area of 150 m^2/g) previous to the impregnation to remove water. The impregnated samples were dried 12–16 hr at approximately 323 K and reduced 14–16 hr at 723 K in flowing hydrogen as previously described (*8, 10*). Extents of reduction to nickel metal were determined by O_2 titration at 673 K (*10*). A brief summary of the physical properties of freshly reduced of Ni/SiO_2 and Ni/Al_2O_3 catalysts is shown in Table 1.

Apparatus and Procedure

Sintering experiments. Prior to sintering, an aliquot (0.5 to 1.0 g) of the previously reduced catalyst was crushed to a fine powder and placed in a quartz reactor cell (*11*) equipped with an in-the-bed thermocouple and designed to facilitate changing from sintering and reduction treatments to high vacuum chemisorption measurements without exposing the sample to air.

The catalyst was re-reduced for 5 hr at 723 K, after which the reactor cell was placed in a tubular quartz furnace and heated to the sintering temperature (923, 973, or 1023 K) by means of a temperature

TABLE 1

Physical Properties of Reduced Supported Nickel Catalysts Before Sintering Treatments

Catalyst	Wt% Ni	BET area[a] (m^2/g)	H_2 uptake[b] (μmol/g)	Percentage reduction[c]
Ni/SiO_2	13.5	199	363	93
Ni/Al_2O_3	15.0	150	200	84

[a] Determined using argon as the adsorbate.
[b] Total H_2 uptake at 298 K.
[c] Determined by O_2 titration at 725 K. (see Ref. *10*).

programmer equipped with proportional temperature control. Hydrogen (99.99%), purified by flowing through a Nix-Ox (Air Products) or a palladium Deoxo Purifier (Englehard) and a dehydrated molecular sieve, was passed continuously through the catalyst bed during the sintering process.

Hydrogen chemisorption measurements. The constant temperature sintering runs were interrupted at specific intervals for hydrogen chemisorption measurements. These measurements were carried out volumetrically using a Pyrex, constant volume chemisorption system capable of a dynamic vacuum of 2×10^{-7} kPa (*11*) according to adsorption procedures described previously (*12*). Room temperature isotherms, obtained by plotting adsorbed micromoles of hydrogen against pressure, were extrapolating to zero pressure to obtain the hydrogen uptake due to chemisorption (*10–12*). Nickel surface areas were calculated assuming one hydrogen atom adsorbed per nickel surface atom and assuming a planar density of $6.77(10^{-2})$ nm^2/nickel atom (*12*). Dispersions and average crystallite diameters were calculated from H_2 uptakes according to Bartholomew and Pannell (*12*).

Electron microscopy. A Hitachi HU-11E transmission electron microscope was used to determine the nickel crystallite size distribution of the catalysts both before and after thermal treatment. The procedure is described elsewhere (*13*).

BET measurements. Initial and final surface areas of the catalyst were determined by employing a BET adsorption technique with argon (Matheson, 99.998%) at liquid nitrogen temperatures. The same chemisorption apparatus (*11*) was used without modification. Extended BET measurements were carried out before and after the sintering experiments at 973 K, to determine changes in the support pore structure that occurred during thermal treatment. The method of calculating the pore size distribution was that proposed by Barrett *et al.* (*14*).

X-Ray diffraction. To determine if there had been a change of support structure or a reaction between the metal and the support during sintering treatments, selected samples were analyzed by means of X-ray diffraction using a Philips diffractometer with graphite monochrometer.

TABLE 2

H_2 Chemisorption and BET Surface Area Data during Sintering of 13.5% Ni/SiO_2 in H_2

Temperature (K)	Time (hr)	H_2 uptake[a] (μmol/g)	BET area[b] (m^2/g)
923	0	353.3	176
	2	311.2	
	6	299.0	
	11	284.4	
	24	268.7	
	32	262.1	
	41	252.9	
	51	251.8	154
973	0	361.0	192
	2	265.8	
	5	239.8	
	9	224.4	
	20	212.8	
	27	209.3	
	35	204.7	
	44	183.9	
	54	175.2	159
1023	0	375.0	231
	2.5	212.6	
	5.5	153.4	
	14	127.2	
	21	125.7	
	31	122.0	
	41	112.6	
	51	98.0	190

[a] Total H_2 uptake measured at 298 K.

[b] BET surface area determined using argon as the adsorbate.

RESULTS

H_2 chemisorption uptakes for Ni/SiO_2 and Ni/Al_2O_3 catalysts during exposure to a H_2 atmosphere at 923, 973, or 1023 K are listed in Tables 2 and 3 while normalized surface areas (H_2 uptakes after sintering for a given time divided by initial uptake) are plotted as a function of time in Figs. 1 and 2. A rapid loss of metal surface area during

TABLE 3

H_2 Chemisorption and BET Surface Area Data for Sintering of 15% Ni/Al_2O_3 in H_2

Temperature (K)	Time (hr)	H_2 uptake[a] (μmol/g)	BET area[b] (m^2/g)
923	0	200.0	142
	2	187.3	
	6	192.8	
	7	191.9	
	12	207.3	
	20	190.8	
	30	185.2	
	40	187.2	
	50	191.4	123
973	0	200.0	155
	2	185.6	
	7	182.8	
	12	183.3	
	20	181.5	
	30	176.4	
	42	172.9	
	50	173.6	133
1023	0	202.0	153
	2	192.2	
	5.75	181.7	
	12	173.0	
	22	165.5	
	30	160.3	
	40	160.0	
	50	151.5	133

[a] Total H_2 uptake measured at 298 K.

[b] BET surface area determined using argon as the adsorbate.

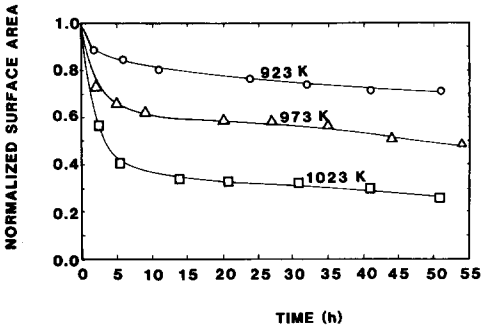

FIG. 1. Hydrogen chemisorption data during sintering of 13.5% Ni/SiO_2 at various temperatures in hydrogen: O, 923 K; △, 973 K; □, 1023 K.

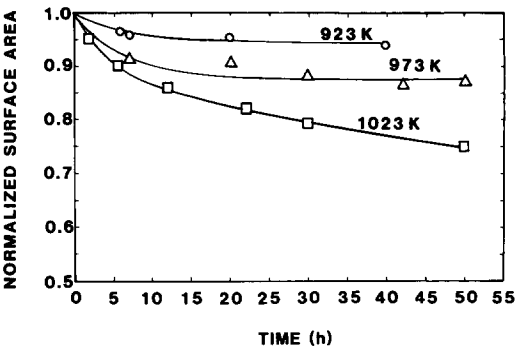

FIG. 2. Hydrogen chemisorption data during sintering of 15% Ni/Al_2O_3 at various temperatures in hydrogen; O, 923 K; △, 973 K; □, 1023 K.

the first 5–10 hr followed by a more gradual decline in area over the next 40–50 hr is evident for both catasysts at any given temperature (see Figs. 1 and 2). The loss of metal surface area clearly increases very significantly with increasing temperature. For example, after 50 hr treatment in H_2 at 923, 973, and 1023 K, Ni/SiO_2 lost about 30, 50, and 70% of its original surface area; the corresponding nickel surface area losses for Ni/Al_2O_3 were 5, 13, and 25%.

Nickel crystallite size distributions obtained from transmission electron microscopy (TEM) for Ni/SiO_2 and Ni/Al_2O_3 cata-

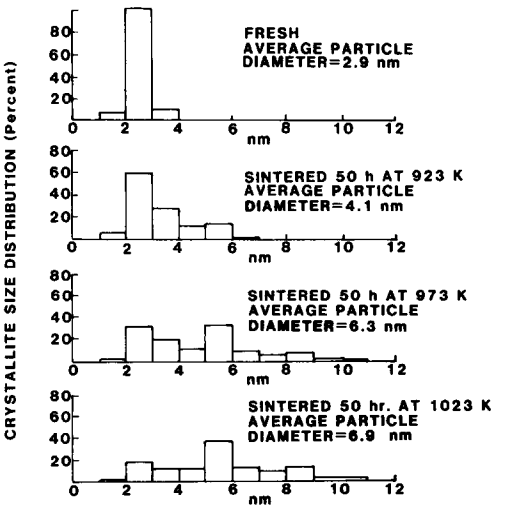

FIG. 3. Crystallite size histograms of 13.5% Ni/SiO_2 after various heat treatments.

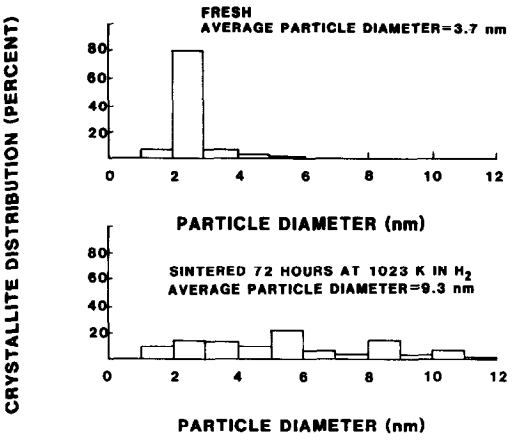

FIG. 4. Crystallite size histograms for fresh and sintered 15% Ni/Al_2O_3.

lysts before and after sintering are shown in Figs. 3 and 4, and typical micrographs for the fresh and sintered catalysts are shown in Fig. 5. The crystallite size distributions are quite narrow for fresh samples of both catalysts; the average particle diameters before sintering of 2.9 and 3.7 nm for Ni/SiO_2 and Ni/Al_2O_3 and particularly the portion of the crystallite size distribution below 4 nm are nearly the same for the fresh samples. After sintering treatments at high temperature, the crystallite size distributions are significantly broadened and shifted to the right; average particle diameters are significantly increased after sintering (see Figs. 3–5). In the case of Ni/SiO_2 the average crystallite diameter increases with increasing temperature of sintering (see Fig. 3).

BET surface areas obtained for fresh and sintered Ni/SiO_2 and Ni/Al_2O_3 catalysts are listed in Tables 2 and 3. Pore size distributions for fresh and 973 K sintered Ni/SiO_2 and Ni/Al_2O_3 samples are plotted in Figs. 6 and 7. Percent losses in BET area for Ni/SiO_2 were 13, 17, and 18% at 923, 973, and 1023 K, respectively. The pore structure was relatively unchanged while pore volume decreased only 12% after sintering 50 hr at 973 K (see Fig. 6). Similar losses in BET area were observed for Ni/Al_2O_3 (13, 14, and 13% at 923, 973, and 1023 K). However, the pore size distribution of Ni/Al_2O_3 was apparently broadened by sintering in H_2 at 973 K (see Fig. 7); nevertheless, there was only about 13% loss of pore volume and the average pore radius remained approximately the same.

X-Ray diffraction scans of Ni/SiO_2 and Ni/Al_2O_3 catalysts after sintering in H_2 atmosphere revealed no evidence of either nickel silicate or nickel aluminate formation. The only major phases observed were nickel metal and γ-alumina (in the case of Ni/Al_2O_3).

The H_2 uptake data from Tables 2 and 3 were fitted to a power law rate model (*15, 16*):

$$-\frac{dD}{dt} = kD^n \qquad (1)$$

where D is dispersion or the fraction of atoms exposed to the surface and n is the order of sintering. According to Wynblatt and Gjostein (*17*), the power law kinetics for sintering can be expressed as:

$$n\ln (D_0/D) = C + \ln t \qquad (2)$$

where C is a constant and t is the sintering time. Thus plots of $\ln (D_0/D)$ versus $\ln t$ should result in straight line plots from which the order of sintering n can be obtained. Plots of $\ln D_0/D$ as a function of $\ln t$ at 923, 973, and 1023 K for Ni/SiO_2 are shown in Fig. 8. Values of n apparently decrease from 15 to 6 with increasing temperature and from 11 to 4 at 973 K with increasing time.

Since values of n were found to vary with temperature and to some extent time, the dispersion vs time data for Ni/SiO_2 and Ni/Al_2O_3 were fitted to the integrated form of Eq. (1),

$$\left(\frac{D_0}{D}\right)^{n-1} = kD_0^{n-1}(n-1)t + 1 \qquad (3)$$

using n values ranging from 2 to 15 to determine rate constants k and activation energies E_a. These values of E_a were compared

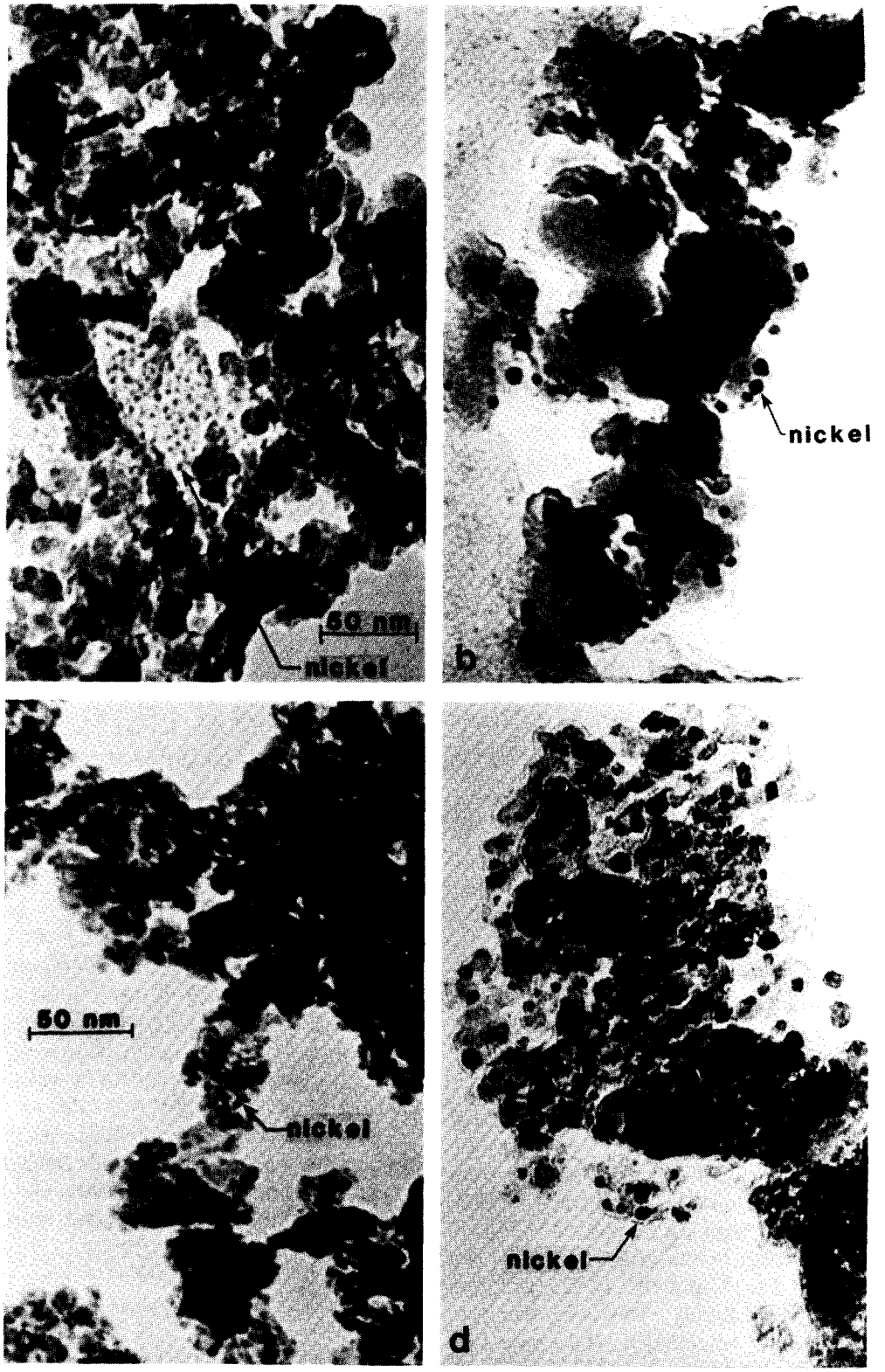

FIG. 5. Electron micrographs of catalysts before and after sintering in H_2 at 1023 K. (a) Fresh 13.5% Ni/SiO_2. (b) Sintered 13.5% Ni/SiO_2. (c) Fresh 15% Ni/Al_2O_3. (d) Sintered 15% Ni/Al_2O_3.

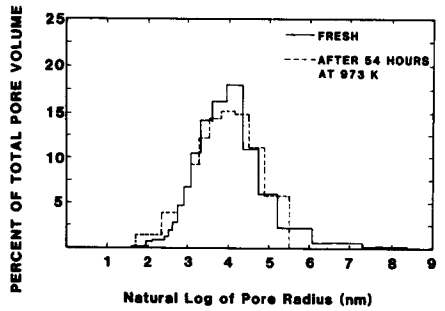

FIG. 6. Comparison of the pore size distribution for 13.5% Ni/SiO_2 before and after sintering at 973 K.

to those obtained from the calculation of apparent activation energies according to Wanke and Flynn (*15*):

$$E_a = R\left(\frac{T_1T_2}{T_2 - T_1}\right)\ln\left(\frac{\Delta t_1}{\Delta t_2}\right) \qquad (4)$$

where Δt_1 and Δt_2 correspond to the time intervals to obtain the same values of D_1 and D_2 at different temperatures T_1 and T_2.

The best overall fit to the dispersion versus time data and the best agreement between values of E_a calculated by the two different techniques was obtained using $n = 7$. Thus linearized power law fits of the data for $n = 7$ are shown in Figs. 9 and 10 for Ni/SiO_2 and Ni/Al_2O_3 catalysts. Kinetic parameters determined from the power law fits and activation energies obtained from Eq. (4) are listed in Table 4. The rate constants for Ni/SiO_2 are smaller than those for Ni/Al_2O_3 at 923 K and larger at 973 and 1023 K. The activation energies for Ni/SiO_2 are significantly larger than for Ni/Al_2O_3. In other words, Ni/SiO_2 is more thermally stable at temperatures less than 923 K; Ni/Al_2O_3 is more thermally stable at higher temperatures.

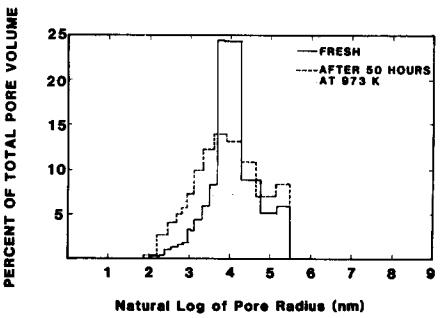

FIG. 7. Comparison of the pore size distribution for 15% Ni/Al_2O_3 before and after sintering at 973 K.

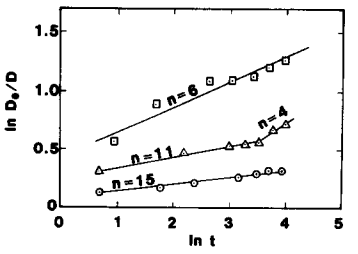

FIG. 8. Plot of ln (D_0/D) vs ln t for 13.5% Ni/SiO_2 during sintering in H_2; ○, 923 K; △, 973 K; □, 1023 K.

DISCUSSION

The Role of Support in Thermal Deactivation of Alumina- and Silica-Supported Nickel

The important question of the role of support collapse in the thermal deactivation of supported nickel was addressed in only three previous studies (*1, 4, 7*). Williams *et al.* (*1*) concluded that loss of nickel surface area occurs during exposure of Ni/Al_2O_3 to H_2/H_2O atmospheres due to loss of fine pore structure and/or conversion of γ-Al_2O_3

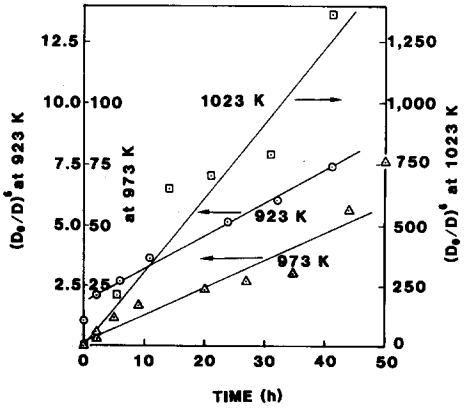

FIG. 9. Linearized power law fit ($n = 7$) for 13.5% Ni/SiO_2; ○, 923 K, △, 973 K, □, 1023 K; linear least-squares correlation coefficients of 0.997, 0.957, and 0.976.

TABLE 4

Kinetic Parameters for Sintering of Ni/Al_2O_3 and Ni/SiO_2 Catalysts in H_2 Atmosphere

Catalyst	Temperature (K)	k^a for $n = 7$ (h^{-1})	Activation energy (kJ)	
			Powerlaw fit[b] ($n = 7$)	Apparent E_a[c]
Ni/Al_2O_3	923	46.3		
	973	91.6	158[d]	149
	1023	344		
Ni/SiO_2	923	17.8		
	973	138	399[e]	368
	1023	2867		

[a] Rate constant from power rate law for $n = 7$ [Eq. (1)].
[b] Activation energy determined from ln k vs $1/T$ where k was determined from power law fit for $n = 7$ [Eq. (3)].
[c] Apparent activation energy estimated from time vs dispersion data using Eq. (4).
[d] Linear least-squares correlation coefficient of 0.979.
[e] Linear least-squares correlation coefficient of 0.991.

to α-Al_2O_3. However, our previous study (*7*) provided evidence that sintering of Ni/γ-Al_2O_3 in H_2 atmosphere results in a 15–25% loss of BET surface area and pore volume while the pore radius is not significantly changed. This suggested a reduction in pore length at constant radius undoubtedly resulting in the blockage of some nickel crystallites. The contribution of support collapse was potentially very significant at sintering temperatures of 923 K and lower; at higher temperatures, the growth of metal crystallites was felt to be a more predominant factor.

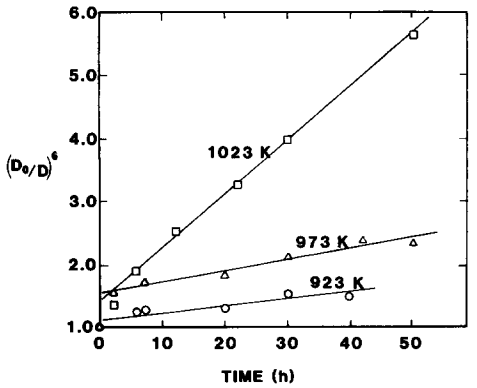

FIG. 10. Linearized power law fit ($n = 7$) for 15% Ni/Al_2O_3; ○, 923 K; △, 973 K; □, 1023 K; linear least-squares correlation coefficients of 0.879, 0.915, 0.995.

The data obtained in this study for Ni/Al_2O_3 are consistent with our previous work (*7*); indeed, percentage losses in nickel surface area of 5–13% at 923 and 973 K are comparable with the observed losses in BET surface area and pore volume (e.g., 14% at 973 K), while the 25% decrease in nickel area at 1023 K is twice as large as the decrease in BET area of 13%. Based on the TEM measurements, the percentage dispersion of Ni/Al_2O_3 decreased from 26 to 10% after sintering at 1023 K compared to a decrease from 19 to 14% based on H_2 adsorption, this agreement again suggesting that loss of nickel surface area due to metal crystallite growth was the predominant mechanism at 1023 K.

In the case of Ni/SiO_2 the combination of H_2 adsorption, TEM, and BET/pore size measurements from this study also provides new insights regarding the contribution of SiO_2 support modifications to thermal deactivation. Although significant decreases in BET area and pore volume of 13–18 and 12% were observed, the much larger decreases of 30–70% in H_2 uptake indicate that the major effect was growth of metal crystallites. This is further substantiated by comparison of the H_2 uptake and TEM data; indeed the 28, 53, and 57% de-

creases in dispersion from TEM correlate very closely with the 30, 50, and 70% decreases in dispersion based on H_2 adsorption—strong evidence that the loss of metal surface area was mainly due to metal crystallite growth.

In their study of very similarly prepared Ni/SiO_2 catalysts treated in He at 873–973 K, Desai and Richardson (*4*) compared nickel surface areas from H_2 adsorption measurements obtained in a flow apparatus with those calculated from magetic measurements. Their conclusion that up to 60–65% of the nickel crystallites were inaccessible due to collapse of the SiO_2 support is not quantitatively consistent with our results which indicate that only 5–20% of the nickel was not available for adsorption of H_2 after sintering. This disagreement is principally a function of differences in the techniques used to measure H_2 adsorption. The flow technique used by Desai and Richardson (*4*) measures irreversible adsorption which varies significantly with metal particle size (*12, 18*) while the measurement of total H_2 uptake by static techniques has been shown to measure monolayer hydrogen coverages reproducibly over a range of nickel crystallite sizes (*12*). Accordingly, we believe the results of this study provide a more quantitative measure of the support contribution for Ni/SiO_2.

Kinetics of Sintering

The kinetic data obtained in this study (Table 4) provide for the first time the capability of modeling quantitatively the thermal deactivation of Ni/SiO_2 and $Ni/\gamma\text{-}Al_2O_3$ catalysts in reducing reaction environments at high temperature. These data may be used, for example, to estimate changes in metal dispersion with time during high temperature methanation, assuming other forms of deactivation are absent or are quantitatively accounted for. Moreover, this study illustrates how kinetic data can be obtained relatively conveniently using H_2 adsorption for purposes of modeling or investigating thermal deactivation.

The data of this study also provide evidence that Ni/SiO_2 prepared by controlled-pH deposition is thermally more stable than $Ni/\gamma\text{-}Al_2O_3$ at low sintering temperatures, i.e., temperatures less than 973 K, while nickel is thermally more stable on the $\gamma\text{-}Al_2O_3$ support at 973 K and higher temperatures. These results in the high temperature range are consistent with previous studies concluding that nickel interacts more strongly with Al_2O_3 compared to SiO_2 since nickel is less readily reduced to the metal in the presence of Al_2O_3 (*8, 10*).

The kinetic data obtained for Ni/SiO_2 in this study showing the order of sintering to decrease as temperature increases and to also decrease with sintering time are in good agreement with results obtained in H_2 atmosphere for a commercial Ni/SiO_2 by Kuo *et al.* (*6*). Thus the results obtained using H_2 adsorption in this study appear to correlate well with the results obtained using X-ray diffraction (XRD). This provides additional support for the conclusion that crystallite growth (rather than support collapse) is the principal mode of thermal deactivation, since XRD analyzes all particles regardless of their accessibility to adsorbing molecules.

The data obtained in this study for sintering of Ni/SiO_2 in H_2 atmosphere, when compared with data obtained in He atmosphere using a catalyst of nearly identical preparation and properties (*3*), enable a valid, quantitative measure of the effects of sintering atmosphere on the rate of nickel crystallite growth. For example, comparison of the normalized surface area data in Fig. 1 of this paper with those in Fig. 4 of Richardson and Crump (*3*) reveals that a 60% loss of surface area occurs in He atmosphere after only 30 hr at 873 K, while only a 30% loss of surface area occurs in H_2 atmosphere at 923 K, some 50 K higher in temperature. Thus the rate of sintering is clearly much higher in He atmosphere in the lower temperature range (i.e., 723–923 K). Nevertheless, comparison of the activation energy for sintering of Ni/SiO_2 in H_2

of 399 kJ/mol (Table 4) to the value of 200 kJ/mol for sintering in He (*3*) indicates that sintering rates should be higher in H_2 atmosphere at sufficiently high temperatures. The significant difference in activation energies for sintering of Ni/SiO_2 in H_2 and He atmospheres also suggests that different sintering mechanisms may operate in the two different atmospheres.

Mechanisms of Crystallite Growth

Two mechanisms of metal crystallite growth have been advanced: (i) crystallite migration (*15, 19–25*) and (ii) atomic migration (*15–17, 26–30*). Crystallite migration involves the migration of entire crystallites over the support surface followed by collision and coalescence. Atomic migration involves detachment of metal atoms from crystallites, migration of these atoms over the support surface, and ultimately capture by larger crystallites.

The identification of the prevailing mechanism is experimentally very difficult (*30, 31*). The following criteria have been used to infer the predominant mechanism:

(i) According to Granquist and Buhrman (*23–25*) crystallite migration results in a log-normal particle size distribution.

(ii) The sintering order n should be between 3 and 5 for atomic migration and between 2 and 13 for crystallite migration (*16, 31*).

(iii) The form of the rate equation for crystallite migration ($-dD/dt = kD^n$) and atomic migration [$-dD/dt = kD^5 \exp(mD/D_0)$] are fundamentally different (*31*).

Unfortunately, the use of these criteria is often ambiguous and controversial. For example, Wanke (*30*) and Kuo and De Angelis (*32*) have taken issue with the conclusion that a log-normal particle size distribution provides unambiguous evidence of crystallite migration. Moreover, Lee (*31*) concludes that the power n in the power rate law expression cannot be used in general to discriminate one mechanism from another. The only sure method involves the direct observation of crystallite migration (*31*).

While the results of this study provide no direct identification of the sintering mechanism, they do suggest a possible shift in sintering mechanism based on the following evidence:

(i) The trend of decreasing n with increasing temperature and time (Fig. 8) is consistent with a shift from crystallite migration controlling at low temperatures and early times to atomic migration controlling at high temperatures and long sintering times. This conclusion is supported by Kuo *et al.* (*6*).

(ii) The crystallite size distribution after sintering at 923 K is clearly log normal and sufficiently narrow to suggest that crystallite migration has occurred. Moreover, the crystallite diameters (3–4 nm) during sintering at 923 K are small enough that crystallite migration is energetically possible (*15*). However, the crystallite size distribution for Ni/SiO_2 at 1023 K is bimodal (perhaps trimodal), very broad, and not in conformance with log normal behavior, suggesting that atomic migration may be operating at the higher temperature. This observation and conclusion find agreement with Kuo and De Angelis (*32*).

(iii) The dispersion-time data in this study were fitted well by the power law rate expression, which is the valid rate expression for crystallite migration (*31*). Attempts to fit the data for Ni/SiO_2 at 973 K to the rate expression for atomic migration (*31*) were unsuccessful.

(iv) The activation energy observed in this study of 150 kJ/mol for Ni/Al_2O_3 is clearly smaller than the energy required for nickel atom detachment of 431 kJ/mol (*3*). Accordingly, the data of this study are consistent with crystallite migration occurring at low temperatures and early sintering times and with atomic migration predominating at high temperatures and long sintering times.

CONCLUSIONS

(1) Loss of nickel surface area occurs during sintering of Ni/SiO_2 and Ni/Al_2O_3 in H_2 as a result of support collapse and

growth of metal crystallites. The contribution of support collapse is more significant in the Ni/Al_2O_3 system and in both systems at low temperatures (e.g., 923 K). At higher sintering temperatures the growth of metal crystallites is the predominant sintering process.

(2) Ni/SiO_2 prepared by controlled pH deposition sinters less rapidly than Ni/γ-Al_2O_3 at temperatures below 923 K. Above 923 K, Ni/SiO_2 sinters more rapidly. The activation energies for sintering of Ni/SiO_2 and Ni/Al_2O_3 in H_2 are 399 and 158 kJ/mol, respectively.

(3) Orders of sintering decrease with increasing temperature and increasing time of sintering in the Ni/SiO_2 and Ni/Al_2O_3 systems.

(4) Sintering of Ni/SiO_2 occurs more rapidly in He atmosphere than in H_2 atmosphere. The activation energies for sintering of Ni/SiO_2 are 200 and 400 kJ/mol in He and H_2 atmospheres.

(5) The data of this study are consistent with a shift in metal sintering mechanism from crystallite migration at low temperatures and sintering times (923 K and 5–20 hours) to atomic migration at higher temperatures and long exposure times (1023 K and 30–50 hours).

ACKNOWLEDGMENTS

We are indebted to Dr. Charles Pitt, University of Utah, for X-ray diffraction measurements and to Mark Jeffrey, Kevin Mayo, Donald Mustard, Gordon Weatherbee, and Travis Bodrero for aid in experimental measurements. The authors gratefully acknowledge financial support from the National Science Foundation (ENG 75-00254) and the Union Oil Foundation.

REFERENCES

1. Williams, A., Butler, G. A., and Hammonds, J., *J. Catal.* **24,** 352 (1972).
2. Bartholomew, C. H., Pannell, R. B., and Fowler, R. W., *Preprints ACS Div. Petroleum Chem.* **22,** (Aug. 1977).
3. Richardson, J. T., and Crump, J. G., *J. Catal.* **57,** 417 (1979).
4. Desai, P., and Richardson, J. T., *in* "Catalyst Deactivation" (B. Delmon and G. F. Froment. Eds.), p. 149. Elsevier, Amsterdam, 1980.
5. Ganasan, P., Kuo, H. K., Saavedra, A., and De Angelis, R. J., *J. Catal.* **52,** 310 (1978).
6. Kuo, H. K., Ganesan, P., and De Angelis, R. J., *J. Catal.* **64,** 303 (1980).
7. Bartholomew, C. H., Pannell, R. B., and Fowler, R. W., *J. Catal.* **79,** 34 (1983).
8. Bartholomew, C. H., Pannell, R. B., and Butler, J. L., *J. Catal.* **65,** 335 (1980).
9. van Dillen, J. A., Geus, J. W., Hermans, L. A. M., and van der Meivben, J., Proc. 6th International Congress on Catalysis, London, 1976.
10. Bartholomew, C. H., and Farrauto, R. J., *J. Catal.*, **45,** 41 (1976).
11. Bartholomew, C. H., Final Report Submitted to ERDA, FE-1790-9, Sept. 6, 1977.
12. Bartholomew, C. H., and Pannell, R. B., *J. Catal.* **65,** 390 (1980).
13. Mustard, D. G., and Bartholomew, C. H., *J. Catal.* **67,** 186 (1981).
14. Barrett, E. P., Joyner, L. G., and Halenda, P. P., *J. Amer. Chem. Soc.* **73,** 373 (1951).
15. Wanke, S. E., and Flynn, P. C., *Catal. Rev.-Sci. Eng.* **12,** 93 (1975).
16. Flynn, P. C., and Wanke, S. E., *J. Catal.* **34,** 400 (1974).
17. Wynblatt, P., and Gjostein, N. A., *Prog. Solid State Chem.* **9,** 21 (1975).
18. Slinken, A. A., Kucherov, A. V., and Rubinshtein, A. M., *Kinet. Catal. (USSR)* **19,** 415 (1978).
19. Ruckenstein, E., and Pulvermacher, B., *AIChE J.* **19,** 356 (1973).
20. Ruckenstein, E., and Pulvermacher, B., *J. Catal.* **29,** 224 (1973).
21. Pulvermacher, B., and Ruckenstein, E., *J. Catal.* **35,** 115 (1974).
22. Ruckenstein, E., and Dadyburjar, D. B., *J. Catal.* **48,** 73 (1977).
23. Granquist, C. G., and Buhrman, R. A., *J. Appl. Phys.* **27,** 693 (1975).
24. Granquist, C. G., and Buhrman, R. A., *J. Appl. Phys.* **47,** 220 (1976).
25. Granquist, C. G., and Buhrman, R. A. *J. Catal.* **46,** 238 (1977).
26. Chakraverty, B. K., *J. Phys. Chem. Solids* **28,** 2401 (1967).
27. Flynn, P. C., and Wanke, S. E., *J. Catal.* **34,** 390 (1974).
28. Wynblatt, P., and Gjostein, N. A., *Acta Met.* **24,** 1165 (1976).
29. Wynblatt, P., *Acta Met.* **24,** 1175 (1976).
30. Wanke, S. E., *J. Catal.* **46,** 234 (1977).
31. Lee, H. H., *J. Catal.* **63,** 129 (1980).
32. Kuo, H. K., and De Angelis, R. J., *J. Catal.* **68,** 203 (1981).